

Article

Theoretical Study on the Structures and Stabilities of $\text{Cu}_n\text{Zn}_3\text{O}_3$ ($n = 1-4$) Clusters: Sequential Doping of Zn_3O_3 Cluster with Cu Atoms

Zhi-Wei Tao ¹, Han-Yi Zou ¹, Hong-Hui Li ¹, Bin Wang ^{1,*}  and Wen-Jie Chen ^{2,*} 

¹ College of Chemistry, Fuzhou University, Fuzhou 350108, China; 211320206@fzu.edu.cn (Z.-W.T.); 221320279@fzu.edu.cn (H.-Y.Z.); 231320203@fzu.edu.cn (H.-H.L.)

² Department of Material Chemistry, College of Chemical Engineering and Materials, Quanzhou Normal University, Quanzhou 362000, China

* Correspondence: wangbin_100@fzu.edu.cn (B.W.); chenwenjie@qztc.edu.cn (W.-J.C.)

Abstract: Density functional theory (DFT) and coupled cluster theory (CCSD(T)) calculations are performed to investigate the geometric and electronic structures and chemical bonding of a series of Cu-doped zinc oxide clusters: $\text{Cu}_n\text{Zn}_3\text{O}_3$ ($n = 1-4$). The structural evolution of $\text{Cu}_n\text{Zn}_3\text{O}_3$ ($n = 1-4$) clusters may reveal the aggregation behavior of Cu atoms on the Zn_3O_3 cluster. The planar seven-membered ring of the CuZn_3O_3 cluster plays an important role in the structural evolution; that is, the Cu atom, Cu dimer (Cu_2) and Cu trimer (Cu_3) anchor on the CuZn_3O_3 cluster. Additionally, it is found that $\text{Cu}_n\text{Zn}_3\text{O}_3$ clusters become more stable as the Cu content (n) increases. Bader charge analysis points out that with the doping of Cu atoms, the reducibility of Cu aggregation (Cu_{n-1}) on the CuZn_3O_3 cluster increases. Combined with the d-band centers and the surface electrostatic potential (ESP), the reactivity and the possible reaction sites of $\text{Cu}_n\text{Zn}_3\text{O}_3$ ($n = 1-4$) clusters are also illustrated.

Keywords: copper-doped zinc oxide clusters; density functional theory; structural evolution; reactivity



Citation: Tao, Z.-W.; Zou, H.-Y.; Li, H.-H.; Wang, B.; Chen, W.-J. Theoretical Study on the Structures and Stabilities of $\text{Cu}_n\text{Zn}_3\text{O}_3$ ($n = 1-4$) Clusters: Sequential Doping of Zn_3O_3 Cluster with Cu Atoms. *Inorganics* **2024**, *12*, 56. <https://doi.org/10.3390/inorganics12020056>

Academic Editor: Graeme Hogarth

Received: 25 December 2023

Revised: 3 February 2024

Accepted: 7 February 2024

Published: 9 February 2024



Copyright: © 2024 by the authors. Licensee MDPI, Basel, Switzerland. This article is an open access article distributed under the terms and conditions of the Creative Commons Attribution (CC BY) license (<https://creativecommons.org/licenses/by/4.0/>).

1. Introduction

Cu-based catalysts have played important roles in industry, such as in electrocatalytic reduction of CO_2 , methanol steam reforming and water gas shift reaction [1–4]. But at the same time, Cu-based catalysts have suffered some restrictions, such as thermal instabilities and low selectivity [1,2]. Sintering and aggregation of the supported Cu nano-particles are considered to be among the reasons for deactivation of Cu-based catalysts [2]. To develop Cu-based catalysts with superior performance, the structure–activity relationship of catalytic active sites and the interaction of the main active component with the additives, including the supports, are the fundamental issues that need to be solved [5]. Cu/ZnO catalysts are among the commonly used Cu-based catalysts, in which Cu usually acts as the main active component and ZnO plays the dual role of promoter and support [6]. Specifically, Cu^{2+} ions would be reduced to the active Cu^0/Cu^+ species, and the addition of ZnO would increase copper dispersion and reducibility, which are related to enhanced catalytic activity [3,7]. Despite great progress, the interaction of the active copper component with other additives, as well as the reaction mechanisms on Cu-based catalysts, are still controversial due to the complexity of the surface [5]. In this context, gas-phase clusters with various sizes, charge states and stoichiometries could unravel the structural characteristics, bonding rules and reactivity of the clusters. Furthermore, the clusters which could emulate specific reactive centers have served as a fruitful tool for providing insight into the reaction mechanism of catalytic materials [8–10].

Additionally, well-supported single-/dual-atom and cluster catalysts have recently become research hotspots [11–15]. Among these, copper oxide clusters have been suggested

to be the catalytic active sites of copper-exchanged zeolites in the methane oxidation to methanol [15]. Herein, copper oxide clusters with different stoichiometries and sizes were embedded in the zeolites channel, and the geometries and stabilities of these clusters and their underlying correlations with the catalytic activities were elaborated. Additionally, a fully exposed Cu_7 cluster anchored to the loop-like [6]cycloparaphenylene was found to be highly active and selective in the CO electroreduction [14]. As for the ZnO clusters, it is accepted that $(\text{ZnO})_n$ ($n < 8$) clusters favored the Zn–O alternating ring structure. As the size (n) of the $(\text{ZnO})_n$ clusters increased to 8, a ring-to-cage transition occurred [16–18]. In these stoichiometric $(\text{ZnO})_n$ ($n = 1$ –13) clusters, $(\text{ZnO})_3$, $(\text{ZnO})_9$ and $(\text{ZnO})_{12}$ were found to possess relatively higher stability [18]. Notably, the discrete Zn_3O_3 cluster is the planar six-membered ring structure, and the wrinkled Zn_3O_3 six-membered ring can be found in the larger $(\text{ZnO})_n$ ($n > 8$) clusters and the common exposed surfaces of hexagonal wurtzite ZnO crystals [17,19–22].

We have constantly strived to explore the novel chemical bonding of gas-phase clusters and to gain further insights into the active sites of complicated catalyst surfaces and the reaction mechanisms of catalytic processes [23–26]. As mentioned above, the sintering and aggregation of the supported Cu nano-particles are among the deactivation reasons for Cu-based catalyst [2]; whereas small-sized supported Cu clusters possess high activity in some reactions [14]. So, it may be interesting to explore the structural evolution and bonding in the $\text{Cu}_n\text{Zn}_3\text{O}_3$ ($n = 1$ –4) clusters via the sequential adding of Cu atoms, as well as the interaction of doped Cu atoms with the Zn_3O_3 cluster. In this work, we make an effort to reveal the evolution rule of the geometric and electronic structures, as well as the chemical bonding in the Cu-doped $\text{Cu}_n\text{Zn}_3\text{O}_3$ ($n = 1$ –4) clusters. Bader charge analysis, d-band center theory and surface electrostatic potential (ESP) are used to analyze the reactivity and reaction sites of $\text{Cu}_n\text{Zn}_3\text{O}_3$ ($n = 1$ –4) clusters. This work may prove enlightening for our future studies on the mechanisms of cluster reactions.

2. Methods

The initial geometries of $\text{Cu}_n\text{Zn}_3\text{O}_3$ ($n = 1$ –4) clusters were constructed using the structural searches of the ABCluster program [27,28] in combination with artificial constructions. These initial geometries were optimized using the B3LYP functional [29–31] in the Gaussian 09 program [32]. The Stuttgart small-core relativistic effective core potential (RECP) was used for the Cu and Zn atoms, whose corresponding basis sets are Cu: [6s,6p,4d,3f,2g]; Zn: [6s,6p,4d,3f,2g] [33–36]. As for O atoms, the aug-cc-pVTZ basis set was adopted [37,38]. In structural optimizations, the vibrational frequencies were calculated to ensure that the optimized structures were free of imaginary frequencies. In order to verify the reliability of the above computational methods (denoted as B3LYP/BS), we compared the bond lengths, binding energies, vibrational frequencies and dipole moments of ZnO and CuO molecules from the available experiments with our calculations. As shown in Table S1, our calculations are in agreement with the data from those experiments. The low-lying isomers within 0.50 eV at the B3LYP/BS level were then subjected to more accurate coupled cluster CCSD(T) single-point-energy calculations using the Molpro 2010 software [39]. Multiwfn program [40,41] was employed to analyze the Bader charge, surface electrostatic potential (ESP) and d-band centers of $\text{Cu}_n\text{Zn}_3\text{O}_3$ ($n = 0$ –4) clusters.

3. Results

It is accepted that the Zn_3O_3 cluster is a planar six-membered ring structure with D_{3h} symmetry (Figure 1a) [16], in which Zn and O atoms are alternately bonded ($d_{\text{Zn-O}} = 1.817 \text{ \AA}$). The distance between two Zn atoms is 2.654 Å.

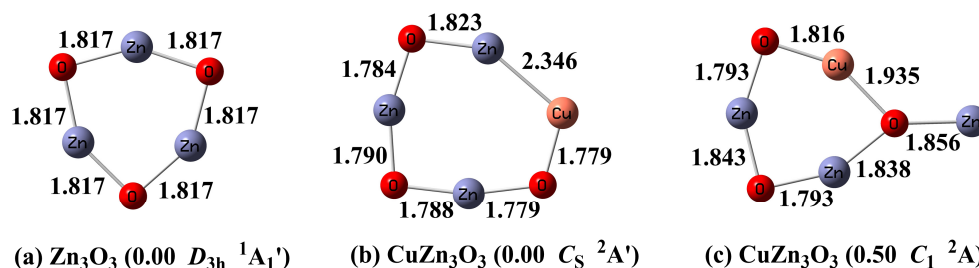


Figure 1. Optimized structures ($\Delta E \leq 0.50$ eV) for Zn_3O_3 and CuZn_3O_3 . The bond lengths are in angstroms and the relative energies (ΔE) in eV are in the parentheses.

3.1. Optimized Structures of CuZn_3O_3

CuZn_3O_3 clusters are constructed by adding a Cu atom to the most stable Zn_3O_3 cluster. The most stable structure of CuZn_3O_3 is shown in Figure 1b, which is consistent with the previous theoretical study [18]. It can be regarded as inserting a Cu atom into the Zn-O bond of the Zn_3O_3 cluster, leading to the planar seven-membered ring structure. The second low-lying isomer (Figure 1c) is 0.50 eV higher in energy, for which the six-membered Zn_3O_3 ring is broken. Other CuZn_3O_3 isomers are higher in energy by at least 0.50 eV. They are collected in the Supporting Information (Figure S1).

3.2. Optimized Structures of $\text{Cu}_2\text{Zn}_3\text{O}_3$

To search for the ground state of the $\text{Cu}_2\text{Zn}_3\text{O}_3$ cluster, a Cu atom was added to the most stable CuZn_3O_3 cluster. The optimized $\text{Cu}_2\text{Zn}_3\text{O}_3$ clusters with relative energy below 0.50 eV are shown in Figure 2. The ground state of the $\text{Cu}_2\text{Zn}_3\text{O}_3$ cluster (Figure 2a) can be viewed as inserting a Cu atom into the Zn-Cu bond of the CuZn_3O_3 cluster, resulting in a planar eight-membered ring structure. It is consistent with the earlier finding of [18] pertaining to the $\text{Cu}_2\text{Zn}_3\text{O}_3$ cluster. The Cu-Cu bond length is 2.366 Å, slightly longer than the Cu-Zn bond length (2.343 Å). This is in agreement with the covalent radius of the Cu and Zn atoms ($d_{\text{Cu}} = 1.52$ Å, $d_{\text{Zn}} = 1.45$ Å) [42] and suggests the metal-metal bonding of the inserting Cu atom with the neighboring Cu and Zn atoms. The second low-lying isomer (Figure 2b), which can be viewed as adding a bridged Cu to the CuZn_3O_3 ground state, is 0.39 eV less stable than the ground state. Other isomers are found to be much higher in energy ($\Delta E > 0.50$ eV). They are collected in the Supporting Information (Figure S2).

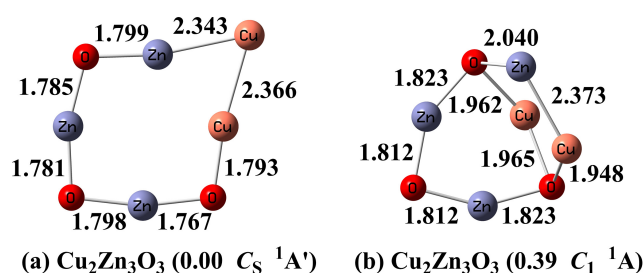


Figure 2. Optimized structures ($\Delta E < 0.50$ eV) for $\text{Cu}_2\text{Zn}_3\text{O}_3$. The bond lengths are in angstroms and the relative energies (ΔE) in eV are in the parentheses.

3.3. Optimized Structures of $\text{Cu}_3\text{Zn}_3\text{O}_3$

As the number of doped Cu atoms increases, more low-lying isomers appear for the $\text{Cu}_3\text{Zn}_3\text{O}_3$ clusters (Figure 3). The most stable $\text{Cu}_3\text{Zn}_3\text{O}_3$ cluster (Figure 3a) can be seen as adding a copper dimer (Cu_2) between two bridged oxygen atoms of the CuZn_3O_3 ground state. At this point, the three-fold coordinated bridged oxygen atom ($\mu_3\text{-O}$) begins to appear in the ground states of $\text{Cu}_n\text{Zn}_3\text{O}_3$ clusters. The Cu-Cu bond length of Cu dimer (Cu_2) is 2.388 Å in the $\text{Cu}_3\text{Zn}_3\text{O}_3$ cluster, which is much longer than that (2.232 Å) of the isolated Cu_2 molecule ($D_{\infty h} \ ^1\Sigma_g^+$) at the same calculation level. It is inferred that there are relatively strong interactions of the Cu_2 moiety with the remaining fragments of $\text{Cu}_3\text{Zn}_3\text{O}_3$.

As shown in Figure 3, there are several isomers that have energies close to the ground state. To further distinguish the stability of these low-lying isomers, single-point CCSD(T) calculations were performed using their B3LYP equilibrium geometries. The single-point CCSD(T) calculations still support the structure contained the Cu₂ (Figure 3a) being the most stable Cu₃Zn₃O₃ cluster (Table S2). Other higher-energy isomers ($\Delta E > 0.50$ eV) are shown in the Supporting Information (Figure S3).

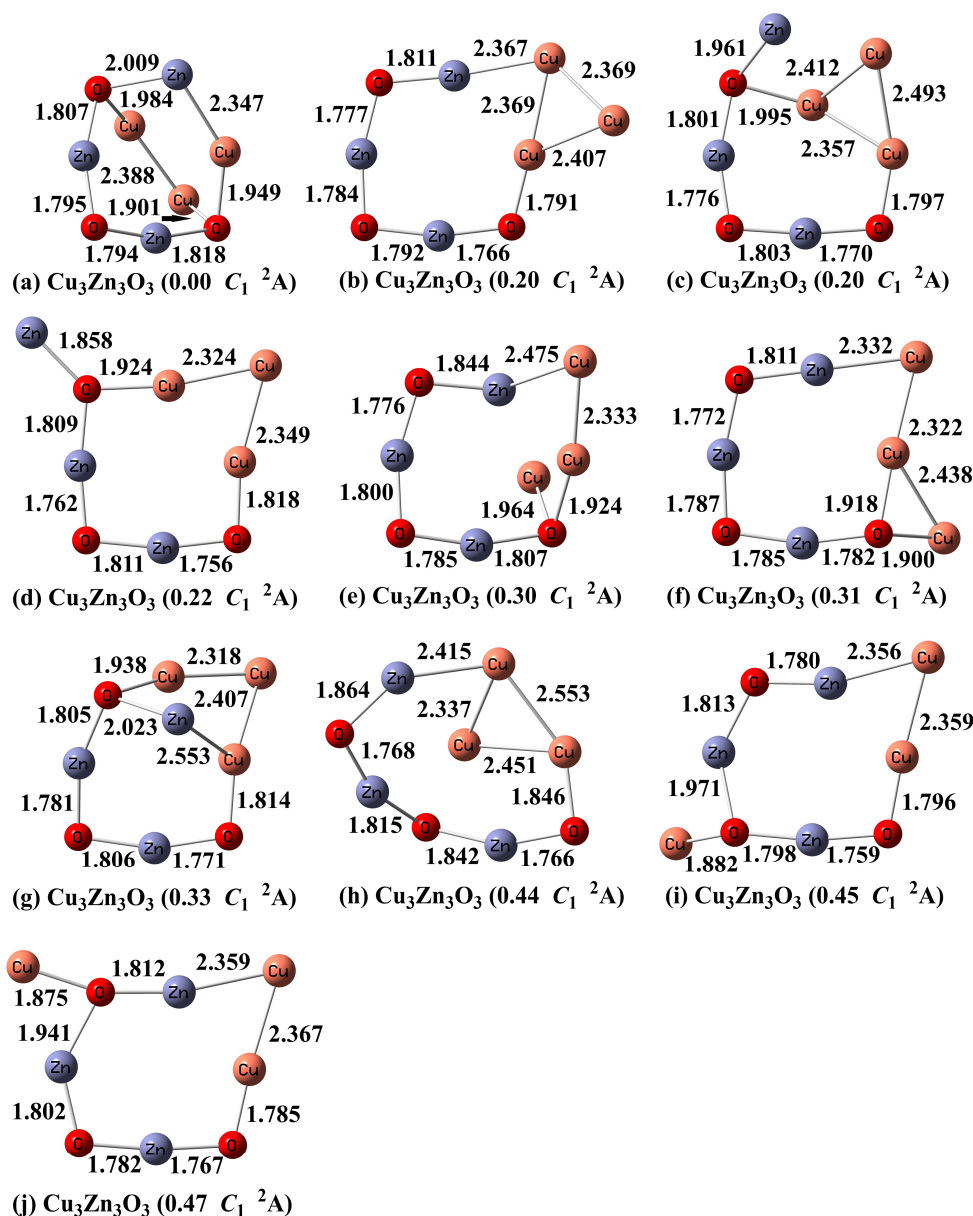


Figure 3. Optimized structures ($\Delta E < 0.50$ eV) for Cu₃Zn₃O₃. The bond lengths are in angstroms and the relative energies (ΔE) in eV are in the parentheses.

3.4. Optimized Structures of Cu₄Zn₃O₃

In our calculations, the most stable Cu₄Zn₃O₃ cluster is shown in Figure 4a. It can be viewed as adding a copper trimer (Cu₃) between two bridged oxygen atoms of the CuZn₃O₃ ground state. Meanwhile, several low-lying isomers within 0.50 eV were found (Figure 4). Among them, there is an isomer (Figure 4b) which contains the Cu₄ moiety and is only 0.10 eV higher in energy. The relative energies of these isomers were further refined by CCSD(T) single-point calculations (Table S2). The CCSD(T) results support the structure shown in Figure 4a being the most stable one, and the isomer shown in Figure 4b is 0.28 eV

less stable. Other higher-energy isomers ($\Delta E > 0.50$ eV) are displayed in the Supporting Information (Figure S4).

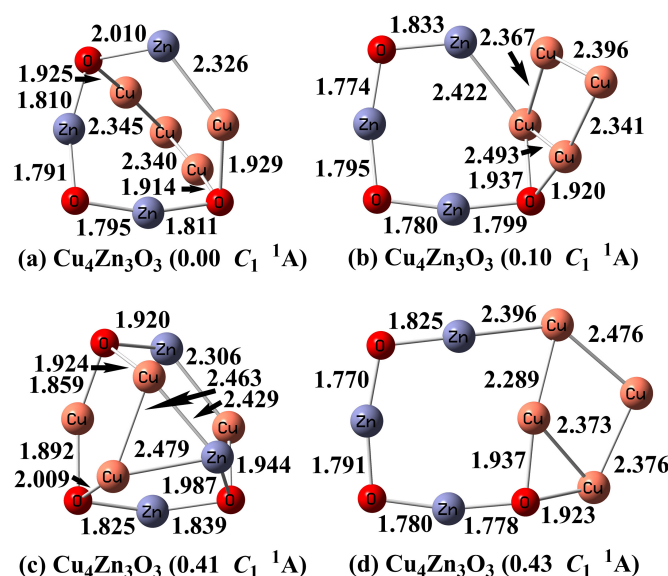


Figure 4. Optimized structures ($\Delta E < 0.50$ eV) for $\text{Cu}_4\text{Zn}_3\text{O}_3$. The bond lengths are in angstroms and the relative energies (ΔE) in eV are in the parentheses.

4. Discussion

4.1. Structural Evolution in $\text{Cu}_n\text{Zn}_3\text{O}_3$ ($n = 1-4$) Clusters and Their Stability

It has been reported that the supported Cu_2 and Cu_3 clusters are the multi-atom cluster catalysts in specific reactions, and appropriate supports could improve their stability and dispersibility [43,44]. Zinc oxides are among the most common promoters and supports for Cu-based catalysts, the Zn_3O_3 six-membered ring is common in the larger $(\text{ZnO})_n$ ($n > 8$) clusters and the wurtzite ZnO [17,19–22]. Studying the structural evolution of the $\text{Cu}_n\text{Zn}_3\text{O}_3$ ($n = 1-4$) clusters via the sequential doping of the Zn_3O_3 cluster with Cu atoms may help us gain insight into the aggregation behavior of Cu atoms on the Zn_3O_3 cluster.

For CuZn_3O_3 , the Cu atom is inserted into the Zn–O bond of the Zn_3O_3 cluster. For $\text{Cu}_2\text{Zn}_3\text{O}_3$, the Cu atom is inserted into the Zn–Cu bond of the CuZn_3O_3 cluster. As for $\text{Cu}_3\text{Zn}_3\text{O}_3$ and $\text{Cu}_4\text{Zn}_3\text{O}_3$ clusters, the planar seven-membered ring of the CuZn_3O_3 cluster starts to play an important role in the subsequent aggregation of Cu atoms (Figure 5); that is, the Cu dimer (Cu_2) and Cu trimer (Cu_3) are attached to the CuZn_3O_3 cluster by two bridged oxygen atoms ($\mu_3\text{-O}$). Herein, we found that at low Cu content ($n = 1, 2$), Cu atoms prefer to insert into the Zn–O bond of Zn_3O_3 first then aggregate to form the ZnCu_2 units. The six-membered ring of Zn_3O_3 gradually expanded to the eight-membered ring of $\text{Cu}_2\text{Zn}_3\text{O}_3$. When the Cu content further increases ($n = 3, 4$), the extra Cu atoms aggregate with each other to form Cu_{n-1} units which are supported on the CuZn_3O_3 cluster.

The relative stability of $\text{Cu}_n\text{Zn}_3\text{O}_3$ ($n = 1-4$) clusters is evaluated via the calculated atomization energy ($E_{b,1}$). The atomization energy ($E_{b,1}$) of $\text{Cu}_n\text{Zn}_3\text{O}_3$ clusters was calculated via the following formula:

$$E_{b,1} = nE(\text{Cu}) + 3E(\text{Zn}) + 3E(\text{O}) - E(\text{Cu}_n\text{Zn}_3\text{O}_3). \quad (1)$$

$E(\text{Cu}_n\text{Zn}_3\text{O}_3)$, $E(\text{Cu})$, $E(\text{Zn})$ and $E(\text{O})$ represent the energy of the $\text{Cu}_n\text{Zn}_3\text{O}_3$ ground state and Cu, Zn and O atoms, respectively. As seen in Table 1, the $E_{b,1}$ increases gradually with the increase in Cu content. This suggests that the $\text{Cu}_n\text{Zn}_3\text{O}_3$ clusters become more stable with Cu atoms doping ($n = 0-4$).

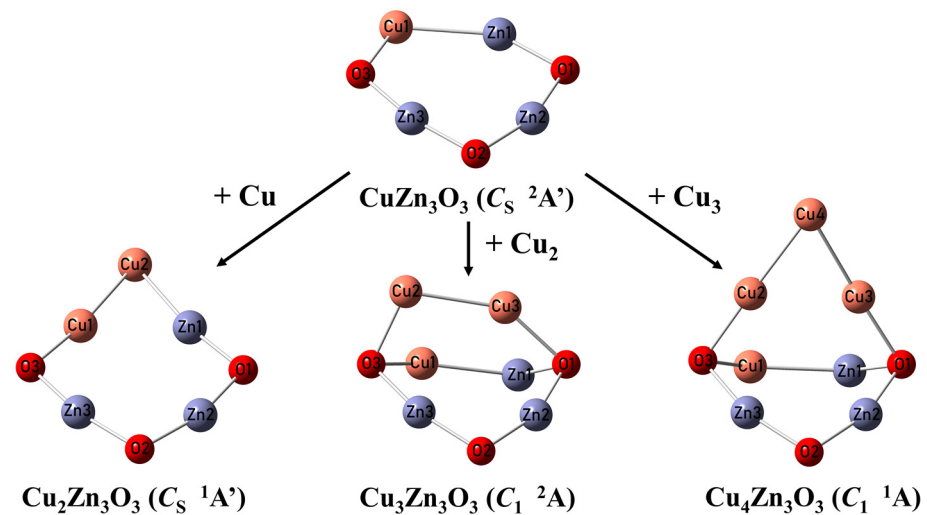


Figure 5. Structural evolution of $\text{Cu}_n\text{Zn}_3\text{O}_3$ ($n = 1-4$) clusters.

Table 1. Atomization energy ($E_{b,1}$) of the $\text{Cu}_n\text{Zn}_3\text{O}_3$ cluster. The energies are in eV.

Cluster	Zn_3O_3	CuZn_3O_3	$\text{Cu}_2\text{Zn}_3\text{O}_3$	$\text{Cu}_3\text{Zn}_3\text{O}_3$	$\text{Cu}_4\text{Zn}_3\text{O}_3$
$E_{b,1}$	22.07	24.03	26.68	28.28	31.27

4.2. Chemical Bonding of $\text{Cu}_n\text{Zn}_3\text{O}_3$ ($n = 1-4$) Clusters

It is known that zinc has the electronic configuration of $3d^{10}4s^2$. Usually, its 3d electrons do not participate in the bonding with other elements. So, in zinc oxides, there is almost an exclusively +2 oxidation state. But copper, as the neighbor element of zinc, has the $3d^{10}4s^1$ configuration, and its 3d electrons participate in the bonding. So, the oxidation state of Cu is more abundant (+1, +2 and +3) [45]. To better understand the charge transfer in the sequential doping of the Zn_3O_3 cluster with Cu atoms, we calculated the Bader charges of the $\text{Cu}_n\text{Zn}_3\text{O}_3$ ($n = 1-4$) clusters (Table 2). For the Zn_3O_3 cluster, the Bader charges of Zn and O atom are +1.13 |e| and −1.13 |e|, respectively. Obviously, the oxidation states of Zn and O in the Zn_3O_3 cluster are +2 and −2, respectively. Thus, the Bader charge of about ±0.5 |e| is indicative of a single-electron transfer, and the Bader charge of about ±1.0 |e| corresponds to a double-electron transfer [46].

Table 2. Bader charges (|e|) analysis of $\text{Cu}_n\text{Zn}_3\text{O}_3$ ($n = 0-4$).

Cluster	Zn-1	Zn-2	Zn-3	O-1	O-2	O-3	Cu-1	Cu-2	Cu-3	Cu-4
Zn_3O_3	1.13	1.13	1.13	−1.13	−1.13	−1.13				
CuZn_3O_3	0.64	1.12	1.15	−1.15	−1.14	−1.06	0.43			
$\text{Cu}_2\text{Zn}_3\text{O}_3$	0.75	1.14	1.12	−1.15	−1.15	−1.10	0.37	0.02		
$\text{Cu}_3\text{Zn}_3\text{O}_3$	0.37	1.11	1.12	−1.16	−1.14	−1.09	0.28	0.25	0.26	
$\text{Cu}_4\text{Zn}_3\text{O}_3$	0.37	1.12	1.11	−1.17	−1.14	−1.11	0.26	0.31	0.31	−0.06

With the Cu atoms doping, the Bader charge of the Zn-1 (as labeled in Figure 5) deviates considerably from +1.0 |e|, and its adjacent Cu atom (denoted as Cu-1) has a Bader charge of less than +0.5 |e|. This suggests an electron transfer between the Zn-1 atom and its adjacent Cu atom (denoted as Cu-1), and the valence state of the Cu-1 atom is $\text{Cu}^{\delta+}$ ($0 < \delta \leq 1$). Additionally, the Bader charges of the different elements seem to be related to the electronegativity (Pauling scale): 1.65 (Zn) < 1.90 (Cu) < 3.44 (O). The charges of Zn are always more positive than those of Cu, and the Cu atom which is bonded to oxygen always has a more positive charge than that of the Cu, which only connects to metal atoms. For example, the Bader charge of the Zn-1 atom in CuZn_3O_3 drops to +0.64 |e| and the charge of the Cu-1 atom is +0.43 |e|. This suggests a charge transfer between the Zn-1

atom and the adjacent Cu-1 atom, and the Cu-1 atom should be Cu^+ . A metal–metal bond is formed between Zn-1 and Cu-1, as indicated by the singly occupied molecular orbital (SOMO) in Figure 6a. On the other hand, the ZnCu unit in CuZn_3O_3 transfers $1.07 |e|$ to the nearby oxygen atoms (denoted as O-1 and O-3) in total. It is inferred that the ZnCu unit in CuZn_3O_3 transfers total two electrons to their adjacent oxygen atoms (O-1 and O-3), which leads to two metal–oxygen single bonds. With continued adding of a Cu atom to the CuZn_3O_3 cluster, the added Cu atom (denoted as Cu-2) inserts into the Zn–Cu bond of the CuZn_3O_3 cluster. As given in Table 2, the Bader charge of Cu-2 in $\text{Cu}_2\text{Zn}_3\text{O}_3$ is only $+0.02 |e|$. This could be understood in terms of the electronegativity discussed above, and the Cu-2 atom may be assigned as Cu^0 . There are metal–metal bonds between Cu-2 and the Zn-1 and Cu-1 atoms, corresponding to the molecular orbital diagrams shown in Figure 6b. Herein, the Bader charge of Zn-1 slightly increases to $+0.75 |e|$, and the charge of the Cu_2 unit is calculated to be $+0.39 |e|$. This suggests more electron transfers between the Zn-1 atom and its adjacent Cu_2 unit. Furthermore, the ZnCu₂ unit in the $\text{Cu}_2\text{Zn}_3\text{O}_3$ cluster transfers $1.14 |e|$ to the adjacent oxygen atoms (O-1 and O-3) in total, which corresponds to two metal–oxygen single bonds. Compared with the Zn_3O_3 cluster, the charges of the other atoms in $\text{Cu}_n\text{Zn}_3\text{O}_3$ ($n = 1,2$) clusters do not change much.

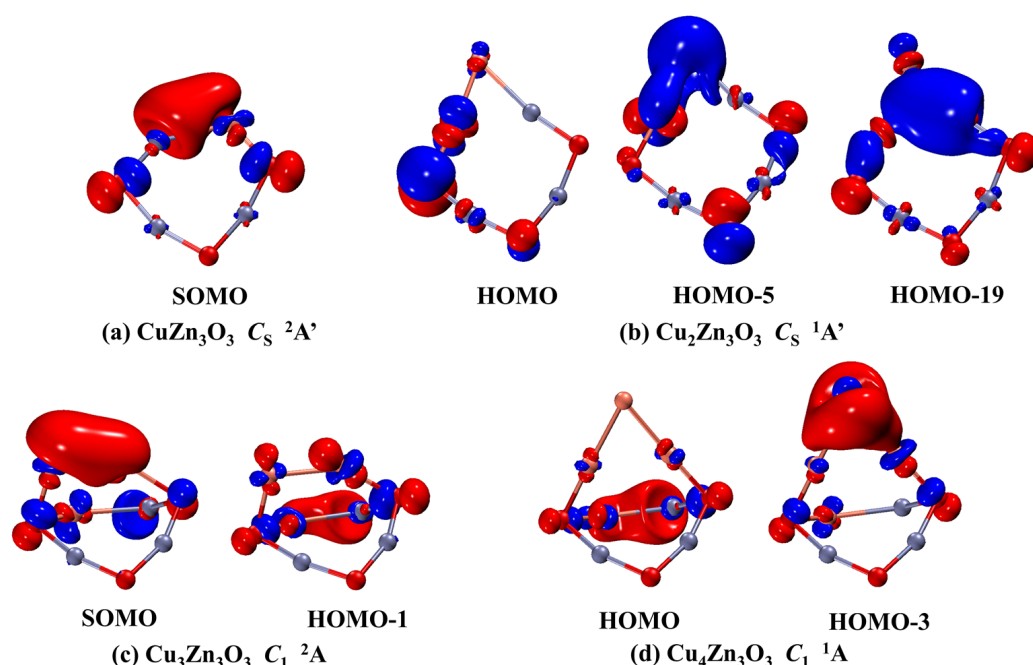


Figure 6. Selected molecular orbitals for the ground-state $\text{Cu}_n\text{Zn}_3\text{O}_3$ ($n = 1-4$) clusters. The red and blue colors stand for different phases of the wave functions.

For $\text{Cu}_n\text{Zn}_3\text{O}_3$ ($n = 3, 4$) clusters, they can be viewed as adding the Cu_2 (Cu-2 and Cu-3) and Cu_3 (Cu-2, Cu-3 and Cu-4) to the CuZn_3O_3 cluster linked by two three-fold coordinated oxygen atoms (O-1 and O-3). As mentioned above, the Bader charges of the Zn-1 and Cu-1 atom in CuZn_3O_3 are $+0.64 |e|$ and $+0.43 |e|$, respectively. But in $\text{Cu}_n\text{Zn}_3\text{O}_3$ ($n = 3, 4$), the charge of Zn-1 reduces to $+0.37 |e|$, and that of Cu-1 also decreases to roughly $+0.3 |e|$. This suggested fewer charge transfers from the ZnCu diatom of $\text{Cu}_n\text{Zn}_3\text{O}_3$ ($n = 3, 4$) to the O-1 and O-3 atoms compared with the charge transfers in the CuZn_3O_3 cluster. Here, the valence state of Cu-1 atom is predicted to be $\text{Cu}^{\delta+}$ ($0 < \delta < 1$). As compensation, the newly added Cu_2 and Cu_3 units in $\text{Cu}_n\text{Zn}_3\text{O}_3$ ($n = 3, 4$) transfer charges of $+0.51 |e|$ and $+0.56 |e|$ to the O-1 and O-3 atoms. As depicted in Figure 6c,d, there are metal–metal bonds in the CuZn unit and in the Cu_{n-1} units of $\text{Cu}_n\text{Zn}_3\text{O}_3$ ($n = 3,4$) clusters. To analyze the interaction of Cu aggregation (Cu_{n-1}) with the CuZn_3O_3 cluster, the binding

energies ($E_{b,2}$) of the isolated Cu_{n-1} clusters with the CuZn_3O_3 cluster were calculated via the following formula:

$$E_{b,2} = E(\text{Cu}_n\text{Zn}_3\text{O}_3) - E(\text{CuZn}_3\text{O}_3) - E(\text{Cu}_{n-1}). \quad (2)$$

$E(\text{Cu}_n\text{Zn}_3\text{O}_3)$, $E(\text{CuZn}_3\text{O}_3)$ and $E(\text{Cu}_{n-1})$ represent the ground-state energy of $\text{Cu}_n\text{Zn}_3\text{O}_3$, CuZn_3O_3 and Cu_{n-1} clusters, respectively. The $E_{b,2}$ of Cu_2 in the $\text{Cu}_3\text{Zn}_3\text{O}_3$ cluster is calculated to be -1.60 eV, and that of Cu_3 in the $\text{Cu}_4\text{Zn}_3\text{O}_3$ cluster is -3.21 eV. The more negative $E_{b,2}$ means a stronger interaction between Cu aggregation (Cu_{n-1}) and the CuZn_3O_3 cluster and a higher stability of Cu_{n-1} on the CuZn_3O_3 seven-membered ring. Here, the more negative binding energies ($E_{b,2}$) coincide with the more transferred charge from Cu_{n-1} to CuZn_3O_3 . For Cu/ZnO catalysts, the addition of ZnO is conducive to increasing the dispersion and reducibility of the active copper component [47]. From the perspective of Bader charge, the Cu_{n-1} in $\text{Cu}_n\text{Zn}_3\text{O}_3$ ($n = 3, 4$) is more reducible than the Cu_n in $\text{Cu}_n\text{Zn}_3\text{O}_3$ ($n = 1, 2$). The synergistic interaction between Cu and Zn in CuZn_3O_3 may enhance the reducibility of Cu species in $\text{Cu}_n\text{Zn}_3\text{O}_3$ ($n = 3, 4$).

4.3. Reactivity of $\text{Cu}_n\text{Zn}_3\text{O}_3$ ($n = 1-4$) Clusters

The model of the d-band center was developed by Nørskov and co-workers [48] and was used as an important descriptor to determine the reactivity of surfaces and clusters [49–53]. The partial density of states (PDOS) for the d-orbitals of metal atoms in $\text{Cu}_n\text{Zn}_3\text{O}_3$ ($n = 0-4$) clusters are depicted in Figure 7, and the d-band centers (ϵ_d) are denoted by the red solid line. For the open-shell systems, the spin up (α) and spin down (β) d-band centers (ϵ_d) were calculated separately (Table S3), and the spin down ones were always higher in energy. So, we uniformly use the spin down d-band centers (ϵ_d) for the subsequent comparison. The energy levels of the highest occupied molecular orbital (HOMO- β) are marked by the blue dashed line. For comparison, all HOMO energy levels in Figure 7 are shifted to zero. As shown in Figure 7f, the ϵ_d moves toward HOMO- β as the Cu content (n) increases. This suggests that the interactions between nucleophilic molecules and the metal atoms become stronger as the Cu content (n) increases [49,52] and also indicates that the reactivity of $\text{Cu}_n\text{Zn}_3\text{O}_3$ ($n = 0-4$) clusters increase as the Cu content (n) increases.

The electrostatic potential (ESP) provides a means of identifying the active sites [49,54]. The surface ESP for $\text{Cu}_n\text{Zn}_3\text{O}_3$ ($n = 1-4$) clusters are shown in Figure 8. Obviously, the red-colored (positive ESP) regions are positioned at the metal atoms, and the ESP of $\text{Cu}_n\text{Zn}_3\text{O}_3$ clusters are less localized compared to the Zn_3O_3 clusters. Additionally, the cyan and yellow tiny spheres in Figure 8 point out the locations of the extreme points of the surface ESP, and the arrows indicate the extreme points with the maximum absolute values. The sites with the most positive values of molecular ESP are associated with the ideal adsorption positions for nucleophilic reagents, whereas the most negative ESP are related to that of electrophilic reagents. In this series of $\text{Cu}_n\text{Zn}_3\text{O}_3$ ($n = 1-4$) clusters, the most-positive regions of ESP are always nearby the Zn-2 atom, except for $\text{Cu}_2\text{Zn}_3\text{O}_3$. Except for $\text{Cu}_2\text{Zn}_3\text{O}_3$, the other $\text{Cu}_n\text{Zn}_3\text{O}_3$ clusters can be viewed as adding the Cu_2 and Cu_3 units to the CuZn_3O_3 cluster linked by two three-fold coordinated oxygen atoms (O-1 and O-3). For $\text{Cu}_2\text{Zn}_3\text{O}_3$, the newly added Cu atom (Cu-2) expands the seven-membered ring of CuZn_3O_3 to the eight-membered ring. The most-positive region of ESP of $\text{Cu}_2\text{Zn}_3\text{O}_3$ is nearby the newly added Cu-2 atom. In $\text{Cu}_n\text{Zn}_3\text{O}_3$ ($n = 1-4$) clusters, the ESP of the three-fold coordinated oxygen atoms is more negative than that of the two-fold coordinated oxygen atoms. For CuZn_3O_3 and $\text{Cu}_2\text{Zn}_3\text{O}_3$, the most-negative regions are located near the O-1 or O-3 atom. For $\text{Cu}_3\text{Zn}_3\text{O}_3$ and $\text{Cu}_4\text{Zn}_3\text{O}_3$, the most-negative regions are located near the O-2 atoms. They indicate the sensitivity of reactivity to the structures.

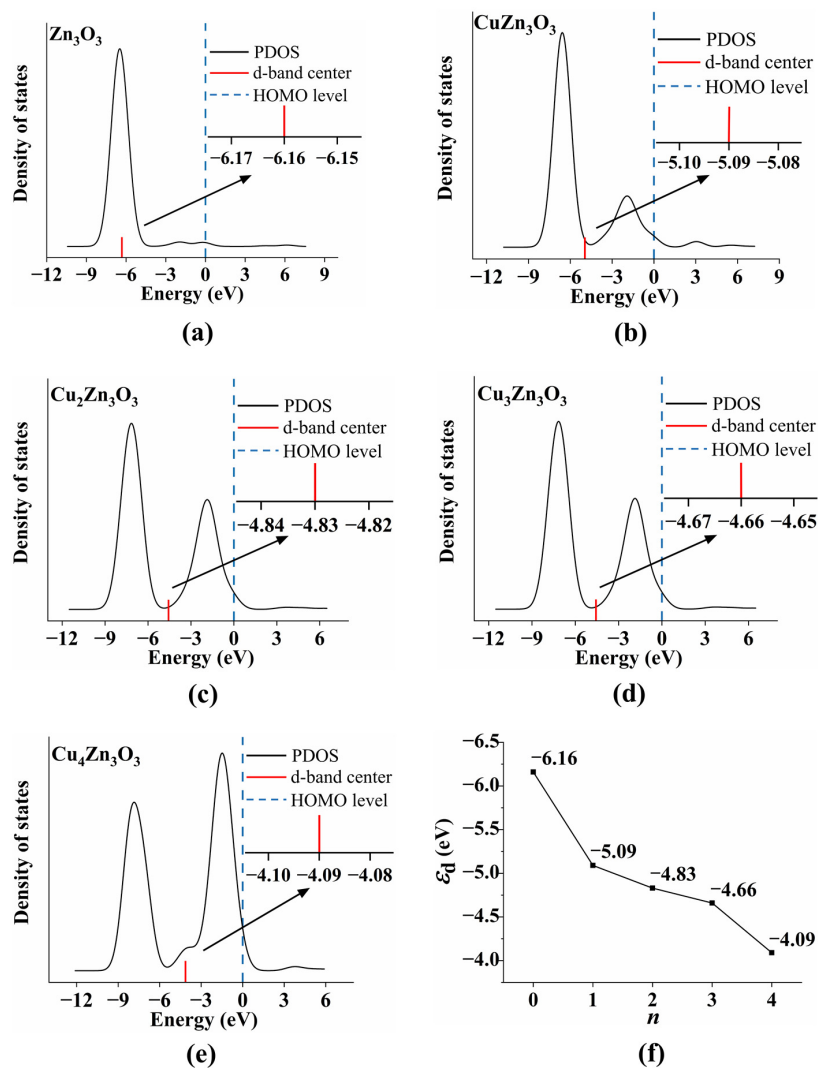


Figure 7. (a–e) The d-band density of states for the lowest-energy $\text{Cu}_n\text{Zn}_3\text{O}_3$ ($n = 0–4$) clusters. The inset is the enlarged drawing of the d-band center. (f) The d-band center (ϵ_d) as a function of Cu content (n) in $\text{Cu}_n\text{Zn}_3\text{O}_3$ ($n = 0–4$) clusters.

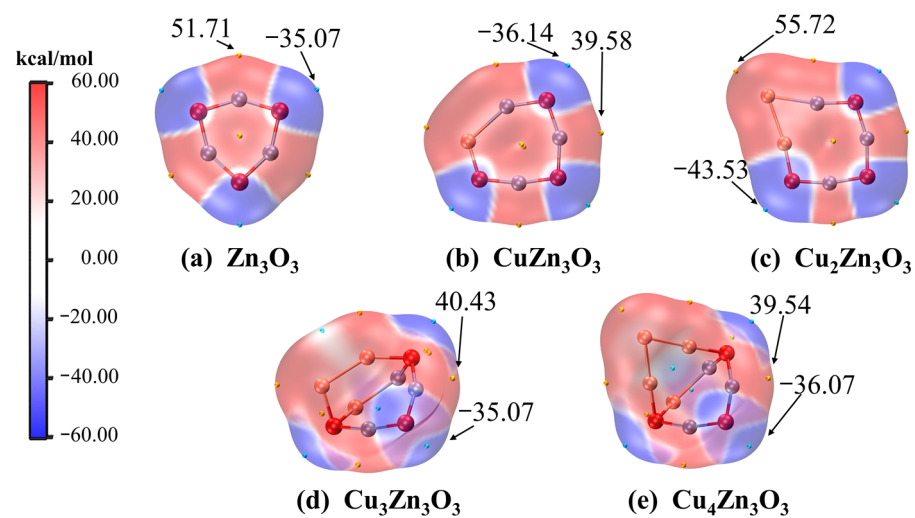


Figure 8. The electrostatic potential (ESP) map on the van der Waals surface for the lowest-energy $\text{Cu}_n\text{Zn}_3\text{O}_3$ ($n = 0–4$) clusters.

5. Conclusions

We report a systematic theoretical study of a series of copper-doped zinc oxide clusters: $\text{Cu}_n\text{Zn}_3\text{O}_3$ ($n = 1-4$). The geometric and electronic structures and the chemical bonding of $\text{Cu}_n\text{Zn}_3\text{O}_3$ ($n = 1-4$) clusters are investigated via extensive density functional theory (DFT) and coupled cluster theory (CCSD(T)) calculations. The structural evolutions of $\text{Cu}_n\text{Zn}_3\text{O}_3$ ($n = 1-4$) clusters are found in our work. At the low Cu content ($n = 1, 2$), Cu atoms prefer to insert into the Zn-O bond of Zn_3O_3 first; then, they aggregate to form the ZnCu_2 units. The six-membered ring of Zn_3O_3 gradually expands to the eight-membered ring of $\text{Cu}_2\text{Zn}_3\text{O}_3$. When the Cu content further increases ($n = 3, 4$), the extra Cu atoms aggregate with each other to form Cu_{n-1} units on the CuZn_3O_3 cluster. Additionally, the relative stability of $\text{Cu}_n\text{Zn}_3\text{O}_3$ ($n = 1-4$) clusters is evaluated. The $\text{Cu}_n\text{Zn}_3\text{O}_3$ clusters become more stable with the doping of Cu atoms ($n = 1-4$). Bader charge analysis suggests that as the Cu content (n) increases, the reducibility of Cu aggregation (Cu_{n-1}) on the CuZn_3O_3 cluster increases. The studies on the d-band centers of $\text{Cu}_n\text{Zn}_3\text{O}_3$ ($n = 0-4$) clusters indicate that the reactivity also increase as the Cu content (n) increases. Information on the possible reaction site of $\text{Cu}_n\text{Zn}_3\text{O}_3$ ($n = 1-4$) clusters are predicted by surface electrostatic potential (ESP) calculations. This work may inspire future studies on the reactions of related clusters.

Supplementary Materials: The following supporting information can be downloaded at <https://www.mdpi.com/article/10.3390/inorganics12020056/s1>. Table S1: Calculated results at the B3LYP/BS level for the bond lengths, binding energies and other properties of ZnO and CuO along with the corresponding available experimental data. Table S2: Relative energies of $\text{Cu}_n\text{Zn}_3\text{O}_3$ ($n = 1-4$) clusters which were further refined by the CCSD(T) single-point calculations. Table S3: The calculated d-band centers for the spin up (α), spin down (β) and both spin modes of $\text{Cu}_n\text{Zn}_3\text{O}_3$ ($n = 0-4$) clusters. Figures S1–S4: Alternative optimized structures for $\text{Cu}_n\text{Zn}_3\text{O}_3$ ($n = 1-4$) clusters at the B3LYP/BS level. Table S4: Cartesian coordinates for the optimized $\text{Cu}_n\text{Zn}_3\text{O}_3$ ($n = 0-4$) clusters. References [55–58] are cited in the Supplementary Materials.

Author Contributions: Investigation, Z.-W.T.; visualization, H.-Y.Z. and H.-H.L.; writing—original draft preparation, Z.-W.T. and H.-Y.Z.; writing—review and editing, B.W. and W.-J.C. All authors have read and agreed to the published version of the manuscript.

Funding: This work was supported by the National Natural Science Foundation of China (NSFC Grant Nos. 21301030 and 21603117).

Data Availability Statement: The data presented in this study are available from the corresponding authors upon reasonable request.

Acknowledgments: The authors gratefully acknowledge supports from the National Natural Science Foundation of China.

Conflicts of Interest: The authors declare no conflicts of interest.

References

1. Xiao, C.; Zhang, J. Architectural Design for Enhanced C_2 Product Selectivity in Electrochemical CO_2 Reduction Using Cu-Based Catalysts: A Review. *ACS Nano* **2021**, *15*, 7975–8000. [[CrossRef](#)] [[PubMed](#)]
2. Ye, R.; Xiao, S.; Lai, Q.; Wang, D.; Huang, Y.; Feng, G.; Zhang, R.; Wang, T. Advances in Enhancing the Stability of Cu-Based Catalysts for Methanol Reforming. *Catalysts* **2022**, *12*, 747. [[CrossRef](#)]
3. Saw, S.K.; Datta, S.; Chavan, P.D.; Gupta, P.K.; Kumari, S.; Sahu, G.; Chauhan, V. Significance and influence of various promoters on Cu-based catalyst for synthesizing methanol from syngas: A critical review. *J. Chem. Technol. Biotechnol.* **2023**, *98*, 1083–1102. [[CrossRef](#)]
4. Teng, M.; Ye, J.; Wan, C.; He, G.; Chen, H. Research Progress on Cu-Based Catalysts for Electrochemical Nitrate Reduction Reaction to Ammonia. *Ind. Eng. Chem. Res.* **2022**, *61*, 14731–14746. [[CrossRef](#)]
5. Ranjekar, A.M.; Yadav, G.D. Steam Reforming of Methanol for Hydrogen Production: A Critical Analysis of Catalysis, Processes, and Scope. *Ind. Eng. Chem. Res.* **2021**, *60*, 89–113. [[CrossRef](#)]
6. Hou, R.; Qiu, R.; Sun, K. Progress in the Cu-based catalyst supports for methanol synthesis from CO_2 . *Chem. Ind. Eng. Prog.* **2020**, *39*, 2639–2647. [[CrossRef](#)]

7. Velu, S.; Suzuki, K. Selective Production of Hydrogen for Fuel Cells via Oxidative Steam Reforming of Methanol over CuZnAl Oxide Catalysts: Effect of Substitution of Zirconium and Cerium on the Catalytic Performance. *Top. Catal.* **2003**, *22*, 235–244. [[CrossRef](#)]
8. Hübner, O.; Himmel, H.-J. Metal Cluster Models for Heterogeneous Catalysis: A Matrix-Isolation Perspective. *Chem. Eur. J.* **2018**, *24*, 8941–8961. [[CrossRef](#)]
9. Yin, S.; Xie, Y.; Bernstein, E.R. Hydrogenation Reactions of Ethylene on Neutral Vanadium Sulfide Clusters: Experimental and Theoretical Studies. *J. Phys. Chem. A* **2011**, *115*, 10266–10275. [[CrossRef](#)]
10. Castleman, A.W., Jr. Cluster Structure and Reactions: Gaining Insights into Catalytic Processes. *Catal. Lett.* **2011**, *141*, 1243–1253. [[CrossRef](#)]
11. Hou, C.-C.; Wang, H.-F.; Li, C.; Xu, Q. From metal–organic frameworks to single/dual-atom and cluster metal catalysts for energy applications. *Energy Environ. Sci.* **2020**, *13*, 1658–1693. [[CrossRef](#)]
12. Qiao, B.; Wang, A.; Yang, X.; Allard, L.F.; Jiang, Z.; Cui, Y.; Liu, J.; Li, J.; Zhang, T. Single-atom catalysis of CO oxidation using Pt₁/FeO_x. *Nat. Chem.* **2011**, *3*, 634–641. [[CrossRef](#)] [[PubMed](#)]
13. Qin, R.; Liu, P.; Fu, G.; Zheng, N. Strategies for Stabilizing Atomically Dispersed Metal Catalysts. *Small Methods* **2018**, *2*, 1700286. [[CrossRef](#)]
14. Liu, Y.-Q.; Qiu, Z.-Y.; Zhao, X.; Wang, W.-W.; Dang, J.-S. Trapped copper in [6]cycloparaphenylene: A fully-exposed Cu₇ single cluster for highly active and selective CO electro-reduction. *J. Mater. Chem. A* **2021**, *9*, 25922–25926. [[CrossRef](#)]
15. Palagin, D.; Knorpp, A.J.; Pinar, A.B.; Ranocchiari, M.; van Bokhoven, J.A. Assessing the relative stability of copper oxide clusters as active sites of a CuMOR zeolite for methane to methanol conversion: Size matters? *Nanoscale* **2017**, *9*, 1144–1153. [[CrossRef](#)]
16. Matxain, J.M.; Fowler, J.E.; Ugalde, J.M. Small clusters of II–VI materials: Zn_nO_i, i = 1–9. *Phys. Rev. A* **2000**, *62*, 053201. [[CrossRef](#)]
17. Fernando, A.; Dimuthu, K.L.; Weerawardene, M.; Karimova, N.V.; Aikens, C.M. Quantum Mechanical Studies of Large Metal, Metal Oxide, and Metal Chalcogenide Nanoparticles and Clusters. *Chem. Rev.* **2015**, *115*, 6112–6216. [[CrossRef](#)] [[PubMed](#)]
18. Yong, Y.; Wang, Z.; Liu, K.; Song, B.; He, P. Structures, stabilities, and magnetic properties of Cu-doped Zn_nO_n (n = 3, 9, 12) clusters: A theoretical study. *Comput. Theor. Chem.* **2012**, *989*, 90–96. [[CrossRef](#)]
19. Tayade, N.T.; Mane, S.M.; Shende, A.T.; Tirpude, M.P.; Shin, J.C. Dissociation of ZnO ring from Zn₃O₃ cluster by CASSCF. *Chem. Phys.* **2021**, *542*, 111077. [[CrossRef](#)]
20. Jin, W.; Chen, G.; Duan, X.; Yin, Y.; Ye, H.; Wang, D.; Yu, J.; Mei, X.; Wu, Y. Adsorption behavior of formaldehyde on ZnO (101[−]0) surface: A first principles study. *Appl. Surf. Sci.* **2017**, *423*, 451–456. [[CrossRef](#)]
21. Cao, Y.; Luo, J.; Huang, W.; Ling, Y.; Zhu, J.; Li, W.-X.; Yang, F.; Bao, X. Probing surface defects of ZnO using formaldehyde. *J. Chem. Phys.* **2020**, *152*, 074714. [[CrossRef](#)]
22. Qiao, L.; Zeng, Y.; Qu, C.Q.; Zhang, H.Z.; Hu, X.Y.; Song, L.J.; Bi, D.M.; Liu, S.J. Adsorption of oxygen atom on Zn-terminated (0001) surface of wurtzite ZnO: A density-functional theory investigation. *Phys. E* **2013**, *48*, 7–12. [[CrossRef](#)]
23. Wang, B.; Xia, C.-J.; Fang, H.-L.; Chen, W.-J.; Zhang, Y.-F.; Huang, X. Mononuclear thorium halide clusters ThX₄ (X = F, Cl): Gas-phase hydrolysis reactions. *Phys. Chem. Chem. Phys.* **2018**, *20*, 21184–21193. [[CrossRef](#)]
24. Wang, B.; Xie, L.; Liu, X.-J.; Chen, W.-J.; Zhang, Y.-F.; Huang, X. Structural Evolution and Chemical Bonding of Di-Niobium Boride Clusters Nb₂B_x^{−/0} (x = 1–6): Hexagonal Bipyramid Nb₂B₆^{−/0} Species. *Eur. J. Inorg. Chem.* **2018**, *2018*, 940–950. [[CrossRef](#)]
25. Wang, B.; Zhang, S.-Y.; Ye, L.-H.; Zhang, X.-F.; Zhang, Y.-F.; Chen, W.-J. Exploring the Reaction Mechanism of H₂S Decomposition with MS₃ (M = Mo, W) Clusters. *ACS Omega* **2020**, *5*, 13324–13332. [[CrossRef](#)] [[PubMed](#)]
26. Wang, B.; Wu, N.; Zhang, X.-B.; Huang, X.; Zhang, Y.-F.; Chen, W.-K.; Ding, K.-N. Probing the Smallest Molecular Model of MoS₂ Catalyst: S₂ Units in the MoS_n^{−/0} (n = 1–5) Clusters. *J. Phys. Chem. A* **2013**, *117*, 5632–5641. [[CrossRef](#)] [[PubMed](#)]
27. Zhang, J.; Dolg, M. ABCluster: The artificial bee colony algorithm for cluster global optimization. *Phys. Chem. Chem. Phys.* **2015**, *17*, 24173–24181. [[CrossRef](#)] [[PubMed](#)]
28. Zhang, J.; Dolg, M. Global optimization of clusters of rigid molecules using the artificial bee colony algorithm. *Phys. Chem. Chem. Phys.* **2016**, *18*, 3003–3010. [[CrossRef](#)]
29. Becke, A.D. A new mixing of Hartree-Fock and local density-functional theories. *J. Chem. Phys.* **1993**, *98*, 1372–1377. [[CrossRef](#)]
30. Lee, C.; Yang, W.; Parr, R.G. Development of the Colle-Salvetti correlation-energy formula into a functional of the electron density. *Phys. Rev. B* **1988**, *37*, 785–789. [[CrossRef](#)]
31. Stephens, P.J.; Devlin, F.J.; Chabalowski, C.F.; Frisch, M.J. Ab Initio Calculation of Vibrational Absorption and Circular Dichroism Spectra Using Density Functional Force Fields. *J. Phys. Chem.* **1994**, *98*, 11623–11627. [[CrossRef](#)]
32. Frisch, M.J.; Trucks, G.W.; Schlegel, H.B.; Scuseria, G.E.; Robb, M.A.; Cheeseman, J.R.; Scalmani, G.; Barone, V.; Mennucci, B.; Petersson, G.A.; et al. *Gaussian 09, Revision C.01*; Gaussian Inc.: Wallingford, CT, USA, 2010.
33. Andrae, D.; Häußermann, U.; Dolg, M.; Stoll, H.; Preuß, H. Energy-adjusted ab initio pseudopotentials for the second and third row transition elements. *Theor. Chim. Acta* **1990**, *77*, 123–141. [[CrossRef](#)]
34. Küchle, W.; Dolg, M.; Stoll, H.; Preuss, H. Energy-adjusted pseudopotentials for the actinides. Parameter sets and test calculations for thorium and thorium monoxide. *J. Chem. Phys.* **1994**, *100*, 7535–7542. [[CrossRef](#)]
35. Cao, X.; Dolg, M. Segmented contraction scheme for small-core actinide pseudopotential basis sets. *J. Mol. Struct. (THEOCHEM)* **2004**, *673*, 203–209. [[CrossRef](#)]
36. Cao, X.; Dolg, M.; Stoll, H. Valence basis sets for relativistic energy-consistent small-core actinide pseudopotentials. *J. Chem. Phys.* **2003**, *118*, 487–496. [[CrossRef](#)]

37. Kendall, R.A.; Dunning, T.H., Jr.; Harrison, R.J. Electron affinities of the first-row atoms revisited. Systematic basis sets and wave functions. *J. Chem. Phys.* **1992**, *96*, 6796–6806. [CrossRef]
38. Dunning, T.H., Jr. Gaussian basis sets for use in correlated molecular calculations. I. The atoms boron through neon and hydrogen. *J. Chem. Phys.* **1989**, *90*, 1007–1023. [CrossRef]
39. Werner, H.J.; Knowles, P.J.; Manby, F.R.; Schütz, M.; Celani, P.; Knizia, G.; Korona, T.; Lindh, R.; Mitrushenkov, A.; Rauhut, G.; et al. MOLPRO, Version 2010.1, a Package of ab initio Programs. Available online: <http://www.molpro.net> (accessed on 1 January 2011).
40. Lu, T.; Chen, F. Multiwfn: A multifunctional wavefunction analyzer. *J. Comput. Chem.* **2012**, *33*, 580–592. [CrossRef]
41. Zhang, J.; Lu, T. Efficient evaluation of electrostatic potential with computerized optimized code. *Phys. Chem. Chem. Phys.* **2021**, *23*, 20323–20328. [CrossRef]
42. Lide, D.R. *CRC Handbook of Chemistry and Physics*, 89th ed.; CRC Press/Taylor and Francis: Boca Raton, FL, USA, 2008.
43. Chen, Z.W.; Yan, J.M.; Zheng, W.T.; Jiang, Q. Cu₄ Cluster Doped Monolayer MoS₂ for CO Oxidation. *Sci. Rep.* **2015**, *5*, 11230. [CrossRef]
44. Chen, Z.W.; Chen, L.X.; Yang, C.C.; Jiang, Q. Atomic (single, double, and triple atoms) catalysis: Frontiers, opportunities, and challenges. *J. Mater. Chem. A* **2019**, *7*, 3492–3515. [CrossRef]
45. Nicholls, D. Copper. In *Complexes and First-Row Transition Elements*; Macmillan Education: London, UK, 1974; pp. 201–206.
46. Thang, H.V.; Pacchioni, G. Spontaneous Formation of Gold Cluster Anions on ZnO/Cu(111) Bilayer Films. *J. Phys. Chem. C* **2019**, *123*, 7644–7653. [CrossRef]
47. Fierro, G.; Lo Jacono, M.; Inversi, M.; Porta, P.; Cioci, F.; Lavecchia, R. Study of the reducibility of copper in CuO-ZnO catalysts by temperature-programmed reduction. *Appl. Catal. A Gen.* **1996**, *137*, 327–348. [CrossRef]
48. Hammer, B.; Nørskov, J.K. Electronic factors determining the reactivity of metal surfaces. *Surf. Sci.* **1995**, *343*, 211–220. [CrossRef]
49. Rodríguez-Kessler, P.L.; Rodríguez-Domínguez, A.R.; Muñoz-Castro, A. On the structure and reactivity of Pt_nCu_n (n = 1–7) alloy clusters. *Phys. Chem. Chem. Phys.* **2021**, *23*, 7233–7239. [CrossRef]
50. Gao, G.; Waclawik, E.R.; Du, A. Computational screening of two-dimensional coordination polymers as efficient catalysts for oxygen evolution and reduction reaction. *J. Catal.* **2017**, *352*, 579–585. [CrossRef]
51. Takagi, N.; Ishimura, K.; Fukuda, R.; Ehara, M.; Sakaki, S. Reaction Behavior of the NO Molecule on the Surface of an M_n Particle (M = Ru, Rh, Pd, and Ag; n = 13 and 55): Theoretical Study of Its Dependence on Transition-Metal Element. *J. Phys. Chem. A* **2019**, *123*, 7021–7033. [CrossRef]
52. Zhang, Q.; Guo, L. Mechanism of the Reverse Water–Gas Shift Reaction Catalyzed by Cu₁₂TM Bimetallic Nanocluster: A Density Functional Theory Study. *J. Clust. Sci.* **2018**, *29*, 867–877. [CrossRef]
53. Megha; Mondal, K.; Ghanty, T.K.; Banerjee, A. Adsorption and Activation of CO₂ on Small-Sized Cu–Zr Bimetallic Clusters. *J. Phys. Chem. A* **2021**, *125*, 2558–2572. [CrossRef] [PubMed]
54. Arteca, G.A.; Hernández-Laguna, A.; Ránde, J.J.; Smeyers, Y.G.; Mezey, P.G. A topological analysis of molecular electrostatic potential on van der Waals surfaces for histamine and 4-substituted derivatives as H₂-receptor agonists. *J. Comput. Chem.* **1991**, *12*, 705–716. [CrossRef]
55. Zack, L.N.; Pulliam, R.L.; Ziurys, L.M. The pure rotational spectrum of ZnO in the X¹Σ⁺ and a³Π_i states. *J. Mol. Spectrosc.* **2009**, *256*, 186–191. [CrossRef]
56. Clemmer, D.E.; Dalleska, N.F.; Armentrout, P.B. Reaction of Zn⁺ with NO₂. The gas-phase thermochemistry of ZnO. *J. Chem. Phys.* **1991**, *95*, 7263–7268. [CrossRef]
57. Huber, K.P.; Herzberg, G. Constants of diatomic molecules. In *Molecular Spectra and Molecular Structure: IV. Constants of Diatomic Molecules*; Huber, K.P., Herzberg, G., Eds.; Springer: Boston, MA, USA, 1979; pp. 8–689.
58. Steimle, T.C.; Nachman, D.F.; Fletcher, D.A. Laboratory measurement of the permanent electric dipole moment of gas-phase CuO in its X²Π state. *J. Chem. Phys.* **1987**, *87*, 5670–5673. [CrossRef]

Disclaimer/Publisher’s Note: The statements, opinions and data contained in all publications are solely those of the individual author(s) and contributor(s) and not of MDPI and/or the editor(s). MDPI and/or the editor(s) disclaim responsibility for any injury to people or property resulting from any ideas, methods, instructions or products referred to in the content.